Self-Propelling Leidenfrost Droplets on a Variable Topography Surface

James M. ARTER[1], David J. CLEAVER[1], Kei TAKASHINA[2], Andrew T. RHEAD[1]
1: Department of Mechanical Engineering, University of Bath, Bath, BA2 7AY, UK
2: Department of Physics, University of Bath, Bath, BA2 7AY, UK

Leidenfrost water droplets can self-propel on heated surfaces with ratcheted topography; a very useful characteristic for systems with excess heat where fluid flow without moving parts is desirable. Reliability and flow rate are significant concerns for such systems. Here, the effect of surface profile on reliability and droplet velocity are investigated on a single device with a continuously adjustable millimetre-scale ratcheted surface. Conditions are described under which the droplet velocity can exceed 350 mm/s. Reliability of droplet propulsion is shown to be improved for ratchet geometries with an overhang.

Droplets on a heated surface in the Leidenfrost regime sustain sufficient vapour flow to levitate them, greatly reducing droplet-surface friction and evaporation time[1]. Asymmetrically ratcheted surfaces channel vapour flow beneath the droplets[2,3] (or sublimating solids such as dry ice[4-6]) asymmetrically enabling them to self-propel.

A recent experimental study[7] has found that qualitatively different behaviour can result from small changes in ratchet geometry. Hence, the effect of surface geometry on propulsion requires investigation. However, experimental work[3,7-9] has generally been limited by the need to fabricate a new surface for every different ratchet geometry. Similarly, theoretical and numerical models describing the physics of propulsion that have appeared in the literature[1,5,7,10-13] have considered only a few specific ratchet profiles. Hence, a comprehensive description of how droplet propulsion depends on ratchet profile is still missing. In a similar vein, recent research has led to proof-of-principle temperature control, power generation and transportation devices[14-16]. Such, and similar future, devices would benefit from increased physical understanding enabling control of flow velocity and improved flow reliability.

To this end, a device is presented whose surface geometry can be adjusted continuously. Data from twenty distinct ratchet configurations are presented, revealing conditions under which droplet velocity can exceed 350mm/s and propel uphill. An overhang geometry is found to significantly improve propulsion reliability. The device [Fig. 1] consists of a frame that enables a stack of rectangular plates of steel to be tilted but also held rigidly. For each plate, two faces are exposed: the edge, and a thin strip on the plate surface between the edge and the neighbouring plate. These faces act as the triangular periodic surface on which droplets are propelled. The angle, α, between the edge-flat and the plate's face is set by locking the plates at a specific incline β and then planarising the surface on a mill. The angle, β, can then be tuned without further machining [Fig. 1(c)] allowing a continuous range of ratchet geometries to be achieved. Slip between plates during device set up

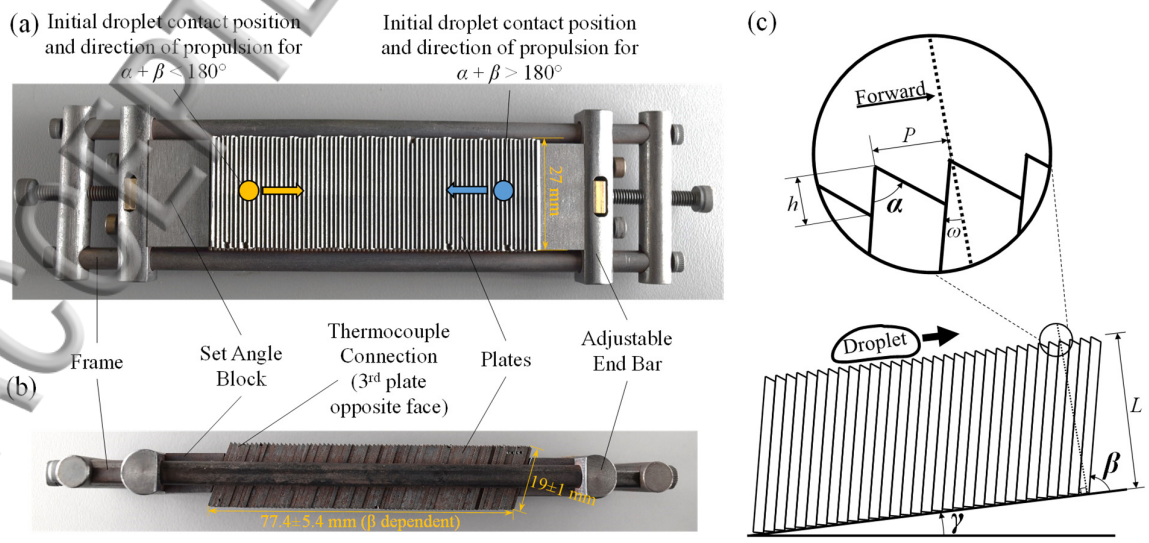

Figure 1. The device is formed of 1 mm thick plates each with an initial height of ~20mm. (a) plan and (b) side views of the device. (c) conveys key variables, ω is negative in this diagram.

This manuscript was accepted by Appl. Phys. Lett. Click here to see the version of record.

inevitably leads to small relative variations in h (average standard deviation of 88μm) and so surface topography was confirmed by contact profilometry [Suppl. Info.]. Individual tooth faces have a roughness of 3.3μm [Suppl. Info.]. Whilst surface roughness is known to have a significant effect on droplet motion[14] this is believed to be secondary to the changing of the surface topography here as the plates have been machined in the same manner each time α is changed. Figure 2 shows how the tooth height, h (see contours), and pitch, P, vary with α and β. Insets (i) to (xx), illustrate the range of periodic surfaces investigated in this study. Shaded regions indicate an overhang geometry – that is, there is space beneath the apex of each tooth, see (ii) and (vii).

During experiments the entire device was placed on a hotplate. Thermocouples inserted into holes drilled into the side of the plates [Fig. 1 (a) & (b)] were used to monitor plate temperature. The hotplate was clamped onto a single axis tilting stage to control the incline, γ, which in turn was mounted on an angle-adjustable stage for fine adjustment. A peristaltic pump was used to dispense 57±3 mg droplets of de-ionised water (giving them a radius slightly below the capillary length of water) at a rate of 4-5 drops per minute whilst the device temperature was slowly increased ($200 < T < 350$°C). Video of each droplet was recorded using a Nikon D750 camera with a 28 mm lens. The position of droplets as a function of time was extracted from the videos via a modified Matlab script[17] which binarises extracted still images and returns the droplet's geometric centre.

Not all droplets followed the intended trajectory. Velocity data were only extracted for droplets propelled across the entire length of the device (in the direction of downward incline of the larger of the two tooth-faces [Fig. 1]). For all droplet paths captured, the droplet initially accelerated rapidly over a few ratchet teeth before reaching an approximately steady velocity [Supp. Info.].

For most surface profiles [Fig. 3] droplet velocity initially increases with temperature, peaks around 270 – 300 °C, and then decreases. This pattern can be broadly explained in terms of four factors: (a) vapour layer thickness; (b) rate and direction of vapour flow; (c) droplet deformation; and (d) wetting contact. That is, in the high temperature limit, deep in the Leidenfrost regime, the vapour layer beneath a droplet is complete and supports the droplet. With reducing temperature, the vapour layer thins leading to stronger interaction with the teeth[8,11]. This can be expected to lead to stronger propulsion as the forwards flow of vapour between the teeth below a

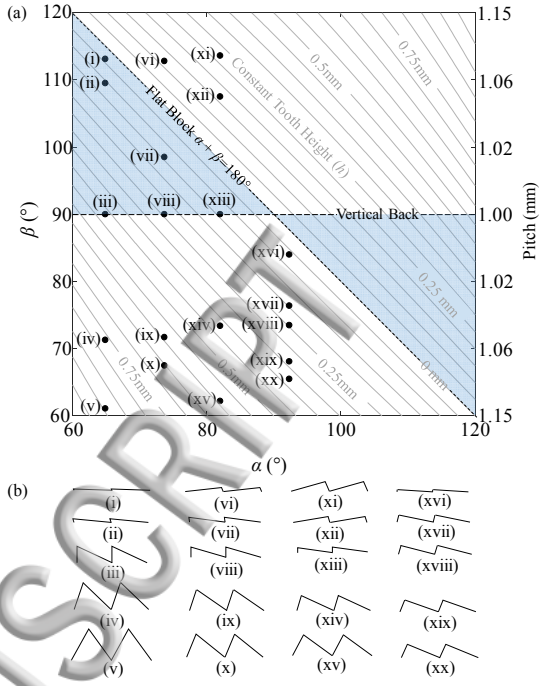

Figure 2. (a) Tooth height and pitch given by varying α and β within the limits of the device. Curves indicate configurations with constant tooth height h. Shaded regions indicate teeth with an overhang geometry. (b) Example tooth geometries from (a).

droplet is closer to its surface (enhancing drag) and more of the flow is in the forwards direction[5,7]. However, droplets also deform further in the ratcheted surface at lower temperatures leading to dissipation of translational kinetic energy (TKE)[18]. In the low temperature limit, with a thin vapour layer, teeth may penetrate the droplet surface and wetting and transition boiling affect droplet dynamics. This can enhance traction[3] but also leads to dissipation of TKE and complications preventing desired propulsion.

Up to a limit, small tooth heights, e.g. (α, β) = (92.3, 84.0), (82.0, 90), (73.7, 98.5), (73.7, 90) and (64.9, 109.5), produce the highest velocities peaking at ~350mm/s in the range 275-300°C. This is higher than previously reported for similar size ratchets[1,2,8] and droplets[11]. This is expected to be due to minimised dissipation of TKE and an optimum ratio of forwards to reverse flow under the droplet. However, data for a very small tooth height, (α, β) = (64.9, 113.1) in Fig. 3 (d), shows a peak velocity at ~230°C. It is assumed this almost flat geometry reaches the Leidenfrost limit at a lower temperature and is unable to create strong propulsive force. For this profile, higher temperatures produce sufficient vapour flow to create a vapour layer thick enough to reduce droplet/teeth interaction. Forward flow is also thought to be reduced owing to increased outflow.

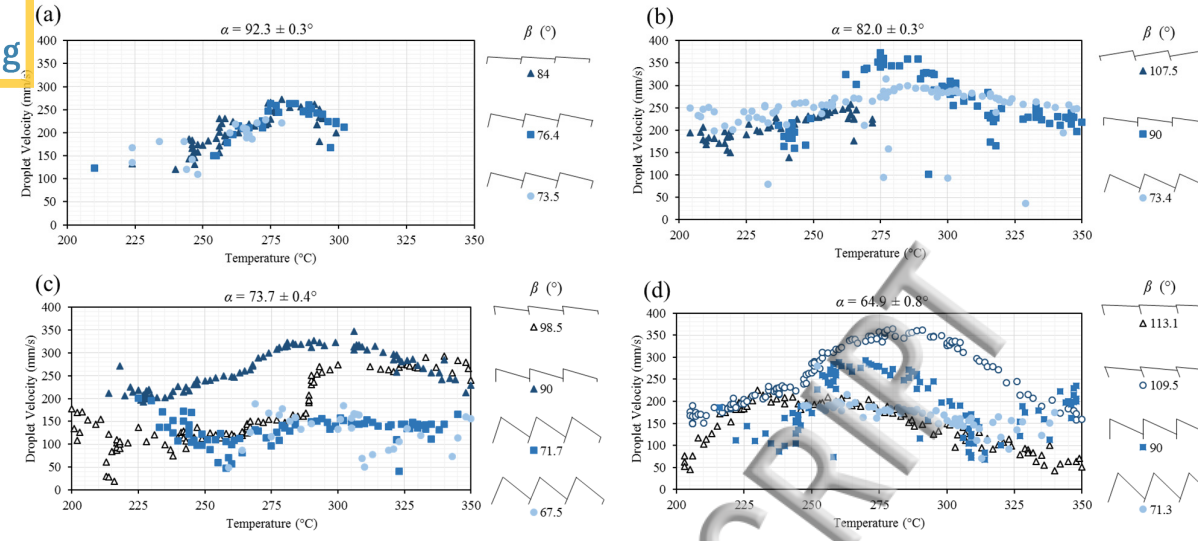

Figure 3. Velocity of propelled droplets for various ratchet profiles. (a) $\alpha = 92.3°$, (b) $\alpha = 82.0°$, (c) $\alpha = 73.7°$ and (d) $\alpha = 64.9°$. Inclination, γ, is 0° for all plots. Open markers denote surfaces with $\omega > 0°$, i.e. overhanging teeth.

Conversely, deep troughs between teeth (largest tooth heights) e.g. $(\alpha, \beta) = (82.0, 73.4)$, (73.7, 71.7 & 76.5), (64.9, 90) and (64.9, 71.3) produced comparatively low velocities and had less reliable behaviour in the low temperature range. This is due to the transition boiling region extending to higher temperatures owing to a thicker vapour layer being required to both prevent penetration of the teeth and to provide sufficient forward flow for propulsion[19].

An overhang profile, described by the angle, ω where $\omega > 0$ indicates overhang, $\omega = 0$ no overhang and $\omega < 0$ anti-overhang (see Fig. 1(c)) can be used to further parametrise teeth. Teeth with $\omega < 0$ generally have a smaller operating temperature range e.g. (α, β) = (92.3, 84.0 & 76.4 & 73.5), (82.0, 107.5 & 73.4), (73.7, 71.7 & 67.5) and (64.9, 71.3) and also exhibit a larger scatter of results hinting at less stable flow dynamics e.g. (73.7, 67.5) and (64.9, 71.3).

Reliability of propulsion (greyscale in Fig.4) is quantitatively assessed by considering the proportion of droplets successfully propelled within a temperature band. Figure 4 shows reliability in seven different temperature bands for α and β axes that map directly onto Figure 2. For no incline ($\gamma = 0°$), data points within the boundaries of the shaded (overhang) region strikingly show 100% reliability. The extent of this reliable region (w.r.t. α and β) is generally greatest in the temperature range 250 - 270°C, shrinking at higher/lower temperatures.

The second and third rows of Figure 4 show data taken at inclines of $\gamma = 2.5°$ and 5°. Consistent with our previous work[3], the temperature range over which propulsion is reliable reduces with increasing incline. Regions where propulsion is maintained with increasing incline correlate with the shaded triangular region (indicating an overhang profile) although the reliable region is reduced.

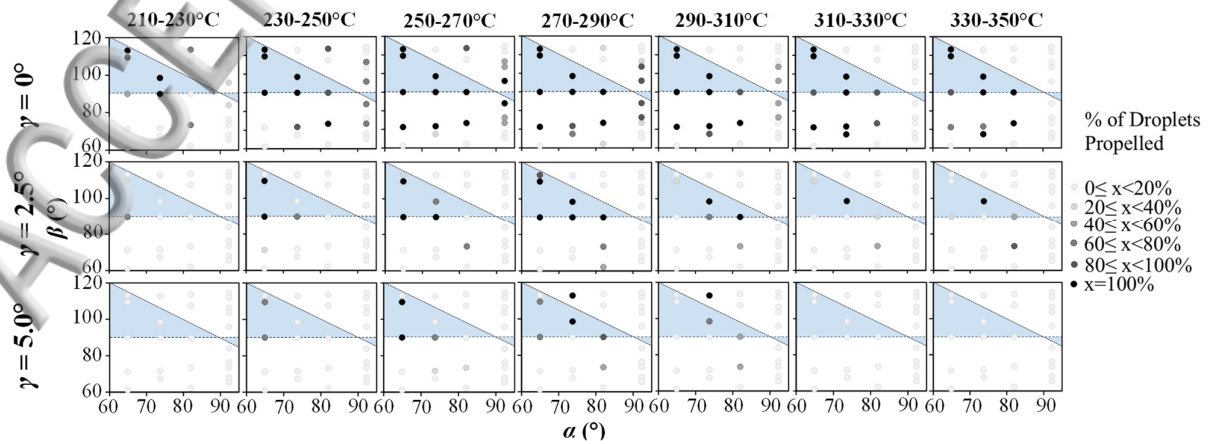

Figure 4. Percentage of droplets propelled for 20 °C temperature bands (columns) and inclinations γ (rows).

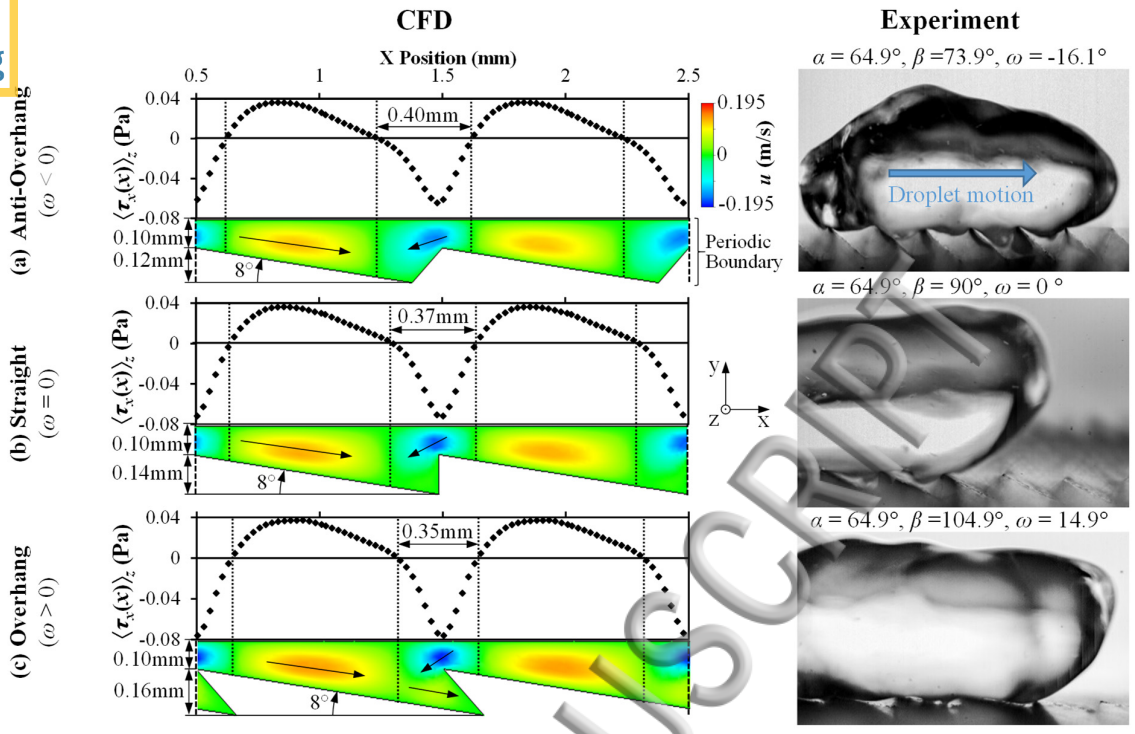

Figure 5. CFD images of flow velocity u in the x-direction and results for $\langle \tau_x(x) \rangle_z$ together with images of droplets for teeth geometries with (a) $\omega < 0$, (b) $\omega = 0$ and (c) $\omega > 0$. CFD data is from a x-y plane halfway between the symmetry plane and the edge of the block. Arrows indicate flow direction.

It is hypothesised that an overhang profile enhances reliability by changing the flow of vapour beneath the droplets[4,5,13] [Fig. 5]. Here, following the work of Cousins et al.[13], an ANSYS™ Computational Fluid Dynamics (CFD) model of an infinitely long but finite width dry ice puck above a ratcheted surface is used to investigate the effect of overhang on general flow behaviour. This puck model specifically removes complications such as droplet surface distortion [Fig. 5], ripples and internal retro-rolling flow leaving purely the effect of vapour flow. The 5mm wide puck has an inlet boundary on the base with a flow rate of CO_2 of 0.15m/s. A symmetry boundary condition at mid-width and periodic boundary conditions in the x-direction (effectively making the puck infinite length) reduce computational effort. Full details of the simulation method are available in Suppl. Info. In order to address the effects of overhang ω, teeth with constant pitch and slope of the longer horizontal surface are considered. ω is varied by changing the slope of the shorter vertical surface [Fig. 5].

The average shear stress, $\langle \tau_i(j) \rangle_k$, shown in Figs. 5 and 6 (b) is the shear stress in the direction i averaged (where $\langle\ \rangle$ is the arithmetic mean) over k for each location j, see supplementary information for details. In Fig. 6 (a) total shear stress, $\langle \tau_x \rangle_{total}$, associated with the viscous force acting on the base of the puck, is calculated by dividing the sum of the x force on the base by the base area.

Comparison of orange areas in Fig. 5 shows that, with increasing overhang, the region of positive u-velocity increases in size as flow propagates into the overhang and the region of negative u-velocity diminishes. As a result, the region of positive shear force increases in size while the region of negative

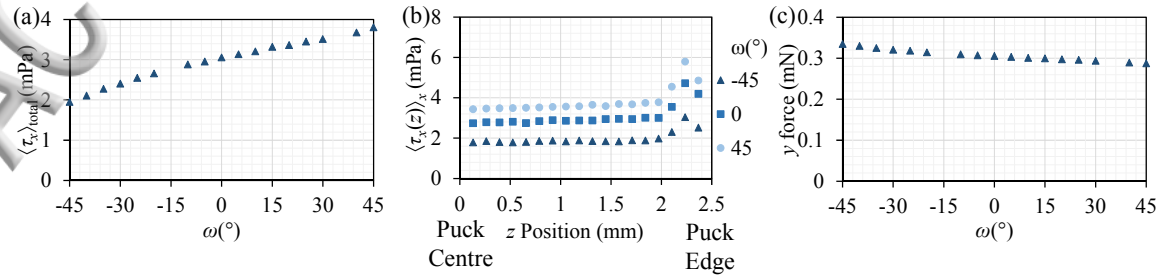

Figure 6. CFD data for (a) $\langle \tau_x \rangle_{total}$ as a function of ω. (b) $\langle \tau_x(z) \rangle_x$ as a function of z position (c) y force as a function of ω.

shear force reduces leading to an increase in total shear force (Fig. 6(a)). Fig. 6 (b) shows this behaviour is consistent across all z locations. Furthermore, Fig. 6(c) shows that as ω increases y force decreases. This is due to the increasing outflow area with increasing ω reducing the magnitude of w-velocity as shown in Fig. S16 in Suppl. Info. The consequent reduction in y-force would result in the distance between the puck / droplet surface reducing until vertical equilibrium is reached likely further increasing x-force. In addition, the reduction in w-velocity will reduce the magnitude of shear in the z-direction, see S17 of Suppl. Info. For the symmetry case this is inconsequential, however when considering reliability, Bouillant et al. have experimentally shown that Leidenfrost droplets can be subject to symmetry breaking resulting from vapour flow[20]. Based on the results presented in Figs 5 and 6, it is hypothesized that overhang could bias the droplet towards propulsion in the x-direction, thereby improving reliability, through three effects: (i) Stronger x-shear force; when the droplet is accelerating from zero velocity the larger u-component of velocity and resulting larger shear force shown in Fig 5(c) creates a strong bias. (ii) Reduced z-shear force; the overhang creates an 'escape route' for flow beneath the droplet that reduces the magnitude of lateral velocity further increasing the relative bias in the x-direction. [Suppl. Info. S16 and S17] (iii) Reduced lateral tilt; the reduced lateral velocity makes it less probable that the droplet will tilt laterally (Bouillant et al.) accelerating the droplet in the z-direction. [Suppl. Info. S17]

To conclude, a device has been demonstrated whose ratcheted surface topography can be changed continuously. Specifically, it enables tooth geometries with overhang. Such tooth profiles, as a consequence of reducing vapour flow in the opposite direction to droplet motion, lead to a dramatic improvement in reliability of propulsion over a wide range of operating conditions, an important feature for future industrial uptake. The device and supporting CFD simulations also highlight the interplay of forward and outward flow enabling the identification of geometries under which droplets self-propel with speeds in excess of 350mm/s.

Supplementary Material

Includes device geometry (S.I.), surface topography (S.II.), experimental procedure (S.III.), data acquisition and analysis (S. IV), further data analysis (S.V) and CFD details (S.VI).

References

1. David Quéré, Annual Review of Fluid Mechanics **45** (1), 197 (2013).
2. H. Linke, B. J. Aleman, L. D. Melling, M. J. Taormina, M. J. Francis, C. C. Dow-Hygelund, V. Narayanan, R. P. Taylor, and A. Stout, Phys Rev Lett **96** (15), 154502 (2006).
3. A. Grounds, R. Still, and K. Takashina, Sci Rep **2**, 720 (2012).
4. T. Baier, G. Dupeux, S. Herbert, S. Hardt, and D. Quere, Phys Rev E Stat Nonlin Soft Matter Phys **87** (2), 021001 (2013).
5. G. Dupeux, M. Le Merrer, G. Lagubeau, C. Clanet, S. Hardt, and D. Quéré, EPL (Europhysics Letters) **96** (5), 58001 (2011).
6. Alois Wuerger, Physical Review Letters **107** (16) (2011).
7. Z. H. Jia, M. Y. Chen, and H. T. Zhu, Applied Physics Letters **110** (9), 5 (2017).
8. Jeong Tae Ok, Eugene Lopez-Oña, Dimitris E. Nikitopoulos, Harris Wong, and Sunggook Park, Microfluidics and Nanofluidics **10** (5), 1045 (2010).
9. G. Dupeux, P. Bourrianne, Q. Magdelaine, C. Clanet, and D. Quere, Sci Rep **4**, 5280 (2014).
10. Guillaume Lagubeau, Marie Le Merrer, Christophe Clanet, and David Quéré, Nature Physics **7** (5), 395 (2011).
11. A. G. Marin, D. A. del Cerro, G. R. B. E. Romer, B. Pathiraj, A. H. in 't Veld, and D. Lohse, Physics of Fluids **24** (12) (2012).
12. Q. Li, Q. J. Kang, M. M. Francois, and A. J. Hu, Soft Matter **12** (1), 302 (2016).
13. Thomas R. Cousins, Raymond E. Goldstein, Justin W. Jaworski, and Adriana I. Pesci, Journal of Fluid Mechanics **696**, 215 (2012).
14. Alexander Cole, Benjamin Jury, and Kei Takashina, Journal of Heat Transfer **137** (3), 034502 (2014).
15. G. G. Wells, R. Ledesma-Aguilar, G. McHale, and K. Sefiane, Nat Commun **6**, 6390 (2015).
16. A. Hashmi, Y. Xu, B. Coder, P. A. Osborne, J. Spafford, G. E. Michael, G. Yu, and J. Xu, Sci Rep **2**, 797 (2012).
17. Mathworks, http://uk.mathworks.com/help/vision/examples/motion-based-multiple-object-tracking.html, Motion Based Multiple Object Tracking [acessed 22/06/18].
18. G. Dupeux, M. Le Merrer, C. Clanet, and D. Quere, Phys Rev Lett **107** (11), 114503 (2011).
19. J. D. Bernardin and I. Mudawar, Journal of Heat Transfer-Transactions of the Asme **121** (4), 894 (1999).
20. Ambre Bouillant, Timothée Mouterde, Philippe Bourrianne, Antoine Lagarde, Christophe Clanet, and David Quéré, Nature Physics (2018).

(a) Initial droplet contact position and direction of propulsion for $\alpha + \beta < 180°$

Initial droplet contact position and direction of propulsion for $\alpha + \beta > 180°$

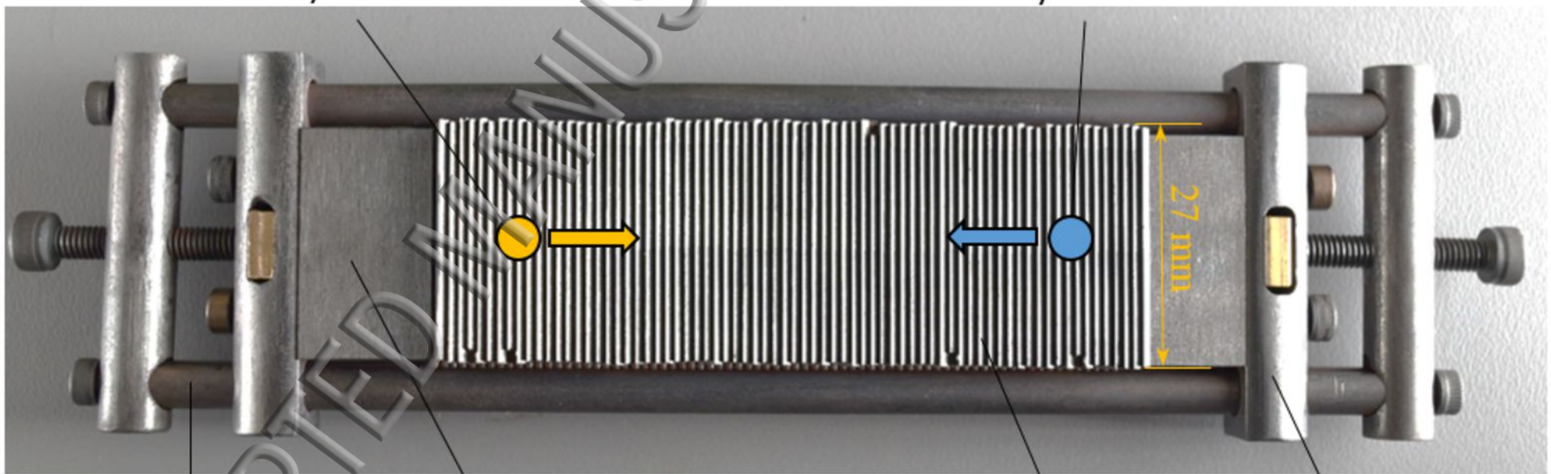

Frame

Set Angle Block

Thermocouple Connection (3rd plate opposite face)

Plates

Adjustable End Bar

(b)

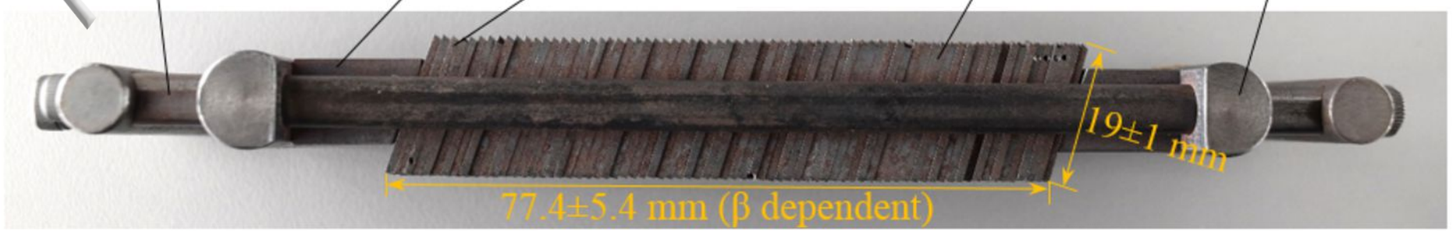

(c)

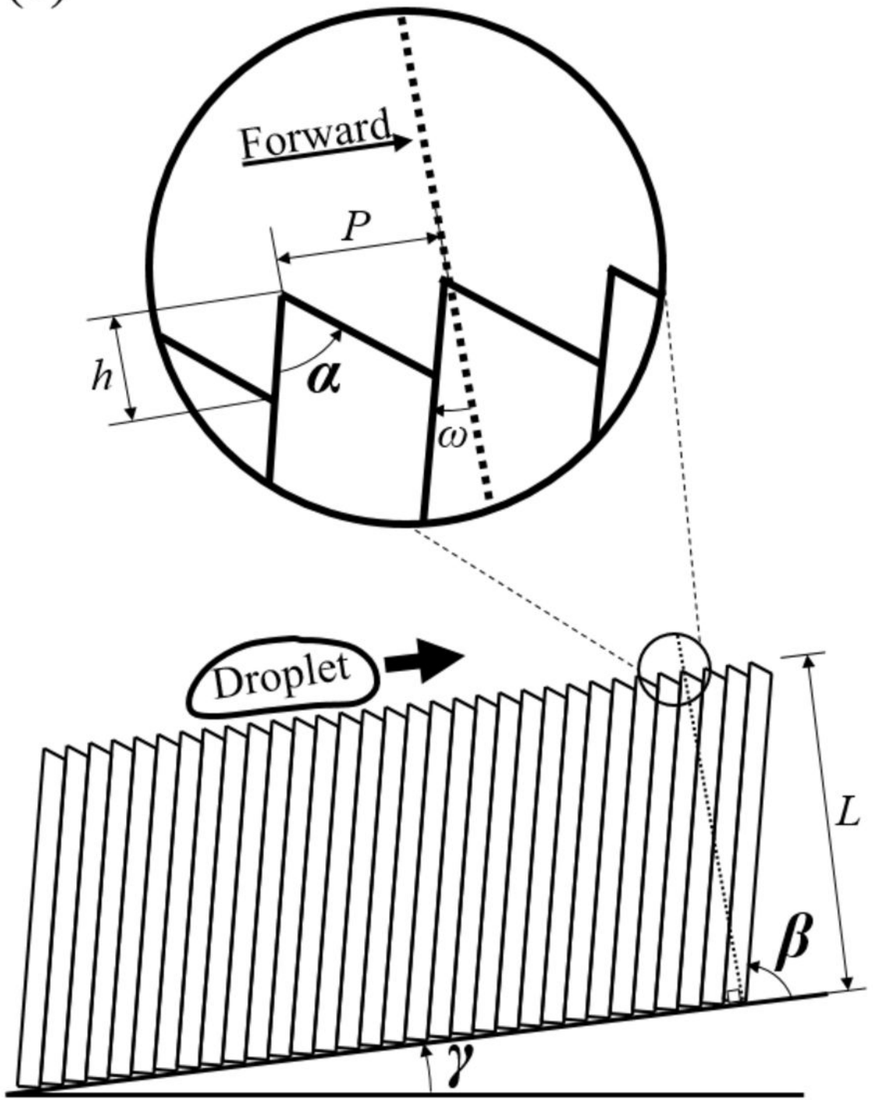

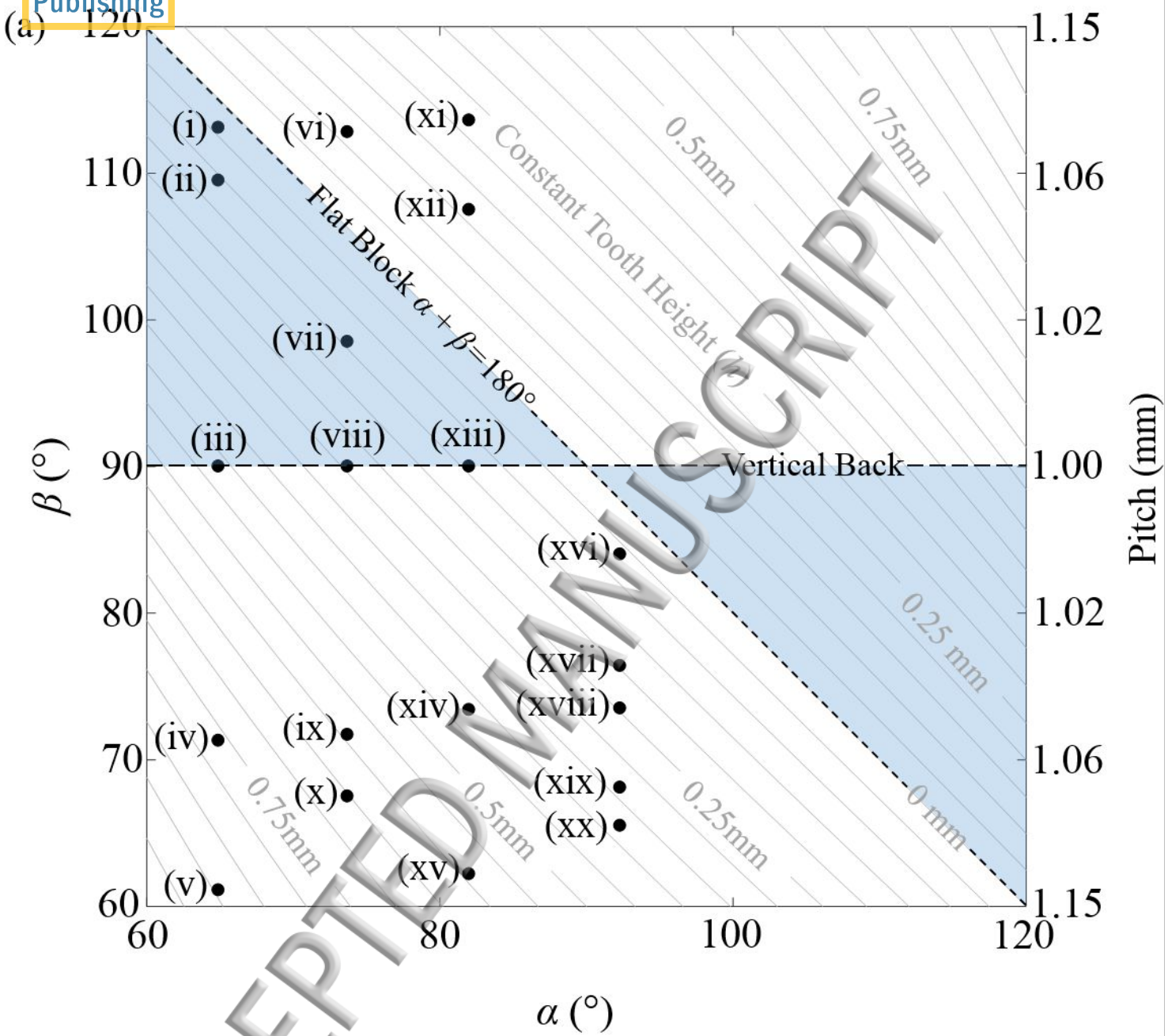

(b)

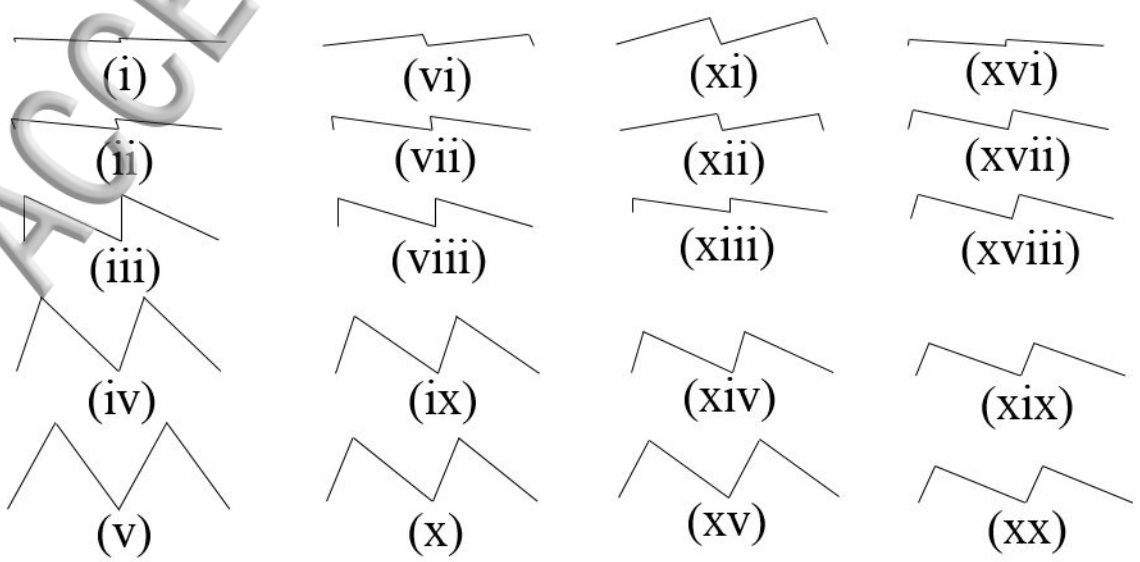

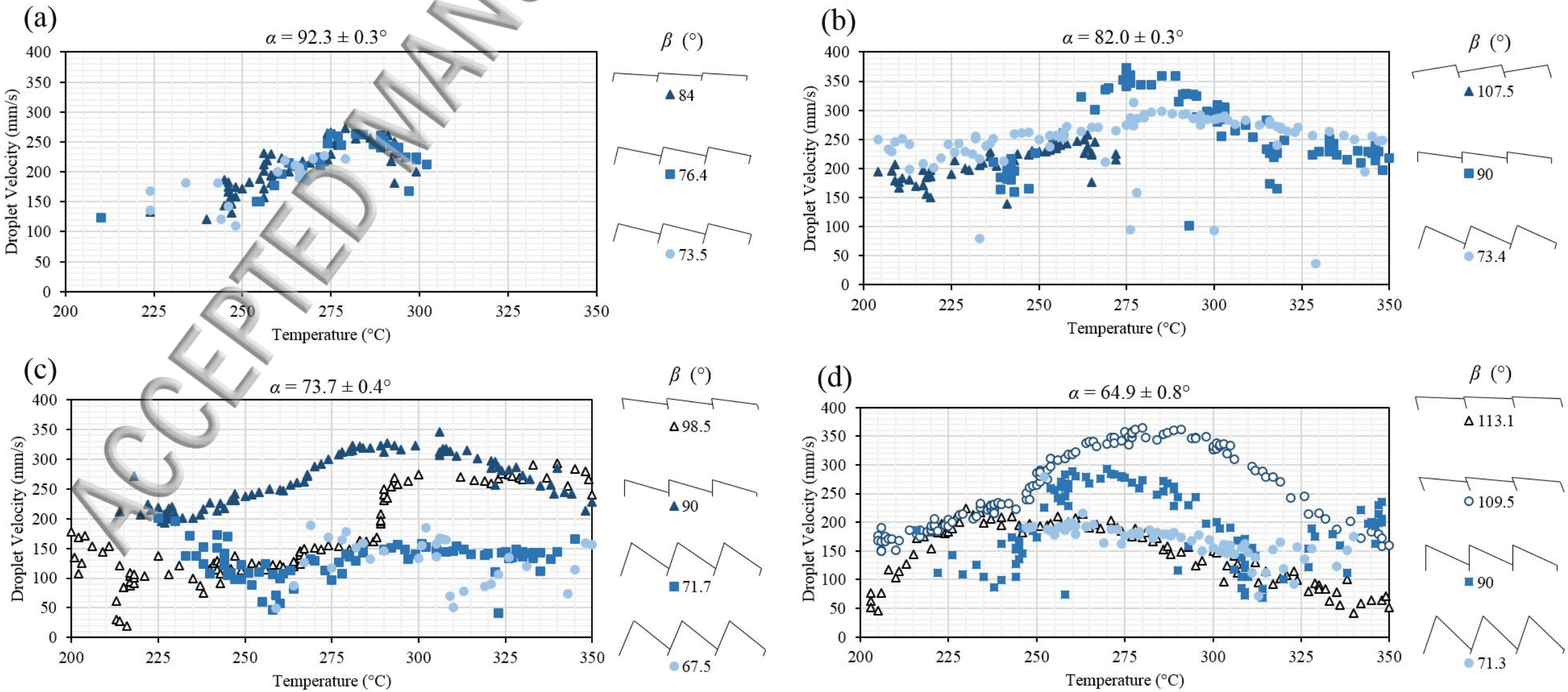

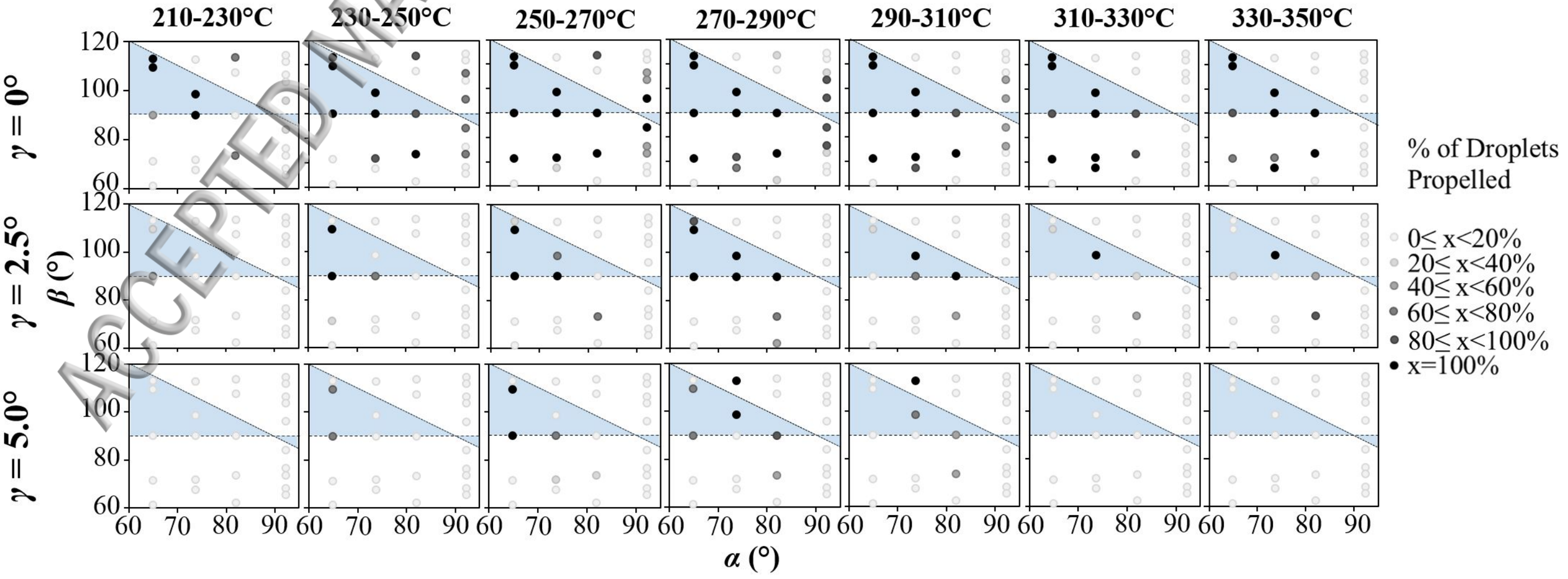

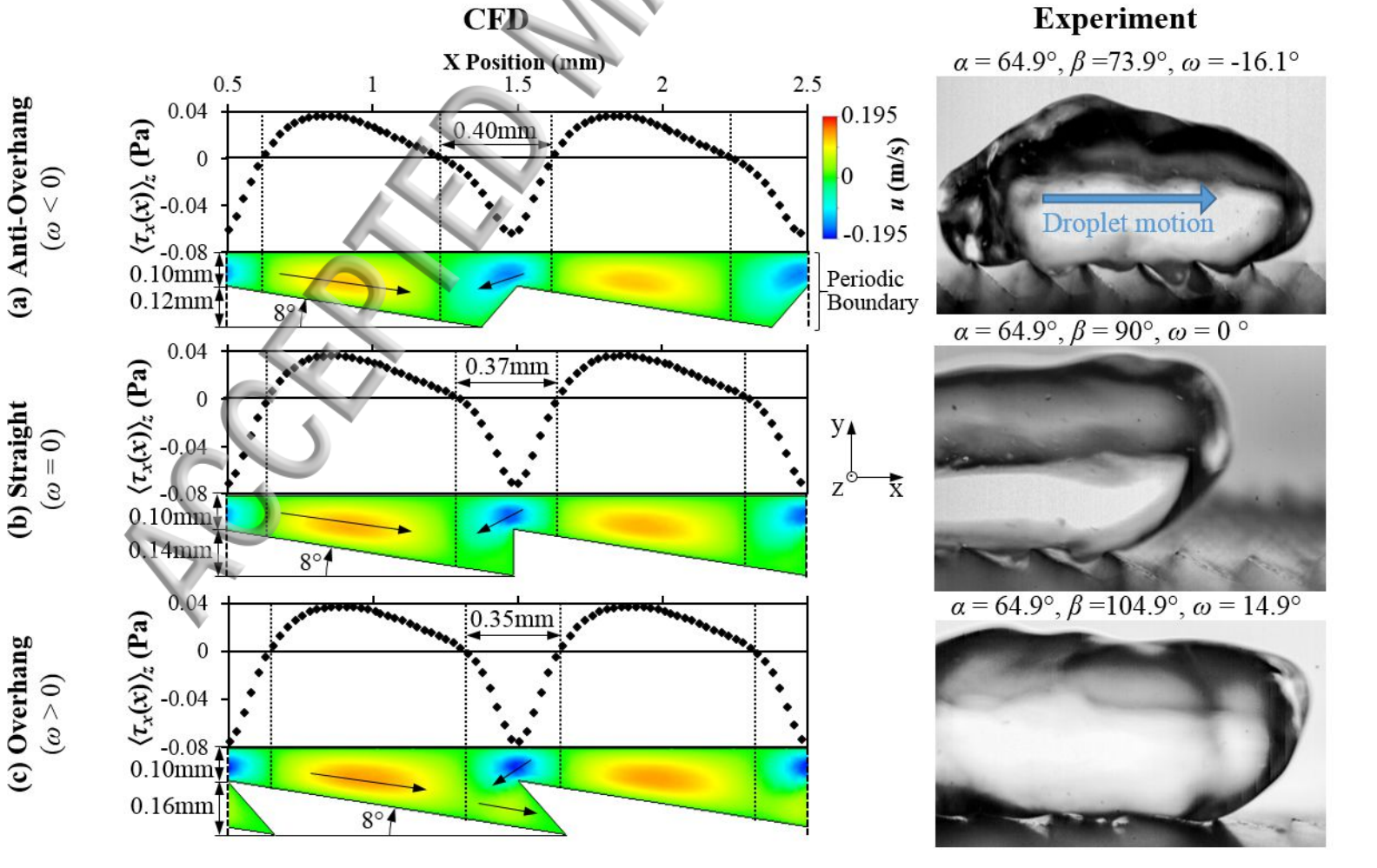

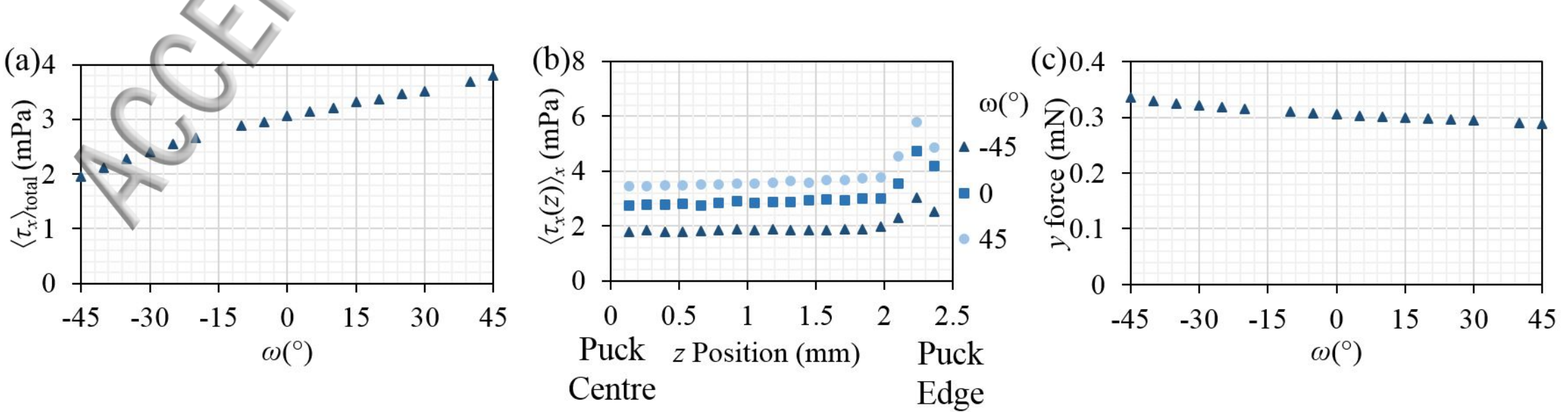
(a)
$\langle\tau_x\rangle_{total}$ (mPa)
0
1
2
3
4
-45
-30
-15
0
15
30
45
ω(°)
(b)
$\langle\tau_x(z)\rangle_x$ (mPa)
0
2
4
6
8
0
0.5
1
1.5
2
2.5
Puck Centre
z Position (mm)
Puck Edge
ω(°)
-45
0
45
(c)
y force (mN)
0
0.1
0.2
0.3
0.4
-45
-30
-15
0
15
30
45
ω(°)